CHEMISTRY OF MATERIALS
Article

Chem. Mater. **2009,** *21,* 3491–3502 3491
DOI:10.1021/cm802949g

Synthesis, Characterization, and Devices of a Series of Alternating Copolymers for Solar Cells

Lars J. Lindgren,[†] Fengling Zhang,[‡] Mattias Andersson,[‡] Sophie Barrau,[‡] Stefan Hellström,[†] Wendimagegn Mammo,[†] Erik Perzon,[†] Olle Inganäs,[‡] and Mats R. Andersson*[,†]

[†]*Department of Chemical and Biological Engineering, Chalmers University of Technology, Polymer Technology, SE-412 96 Göteborg, Sweden, and* [‡]*Biomolecular and Organic Electronics, IFM, Linköping University, SE-581 83 Linköping, Sweden*

Received October 29, 2008. Revised Manuscript Received May 25, 2009

In this study we report the synthesis, characterization, and photovoltaic properties of a series of six conjugated polymers based on donor−acceptor−donor (DAD) structure. The polymers are obtained via Suzuki polymerization of different alkoxy-substituted DAD monomers together with a substituted fluorene or phenylene monomer. Application of polymers as light-harvesting and electron-donating materials in solar cells, in conjunction with both [60]PCBM and [70]PCBM as acceptors, show power-conversion efficiencies (PCEs) up to 2.9%, values obtained without extensive optimization work. Furthermore, atomic force microscopy and field-effect transistor (FET) mobility measurements of acceptor−polymer mixtures show that differences in substitution on the polymers affect morphology, mobility, and device performance. Within the series of polymers, all showing similar optical absorption and redox behavior, substituents play an important role in phase separation on a micrometer scale, which in turn has a large impact on device performance. The phase-separation behavior is clearly seen in [70]PCBM devices where the best-performing devices are obtained using the polymers with short alkoxy groups or no substituents together with a high speed of spin coating during device preparation.

Introduction

In the past few decades, extensive research has been conducted on conjugated polymers for electronic applications. Solar cells, with conjugated polymers as the active, light-harvesting materials, can be distinguished as one of the most important applications. Power-conversion efficiencies (PCEs) up to 5% have been reported for polymer solar cells, with conjugated polymers as electron-donating material and [6,6]-phenyl-C_{61}-butyric acid methyl ester, [60]PCBM,[1] as electron acceptor.[2−4] Recently, using the acceptor [70]PCBM and the polymer PCPDTBT, it was shown that the power-conversion efficiency could be increased from 2.8% to 5.5% by addition of alkanedithiols during spin-casting.[5] However, to further increase the performance of polymer solar cells and make them more competitive, a lot of work is yet to be done. Solely high power-conversion efficiency will not bring the polymer solar cells to commercialization. Issues like operational stability and large area/industrial processing are extremely important for the future of this technology and need to be studied further.[6,7] In the development of new materials it is central to find significant relationships between molecular structure and device performance. Three properties, that is, the open-circuit voltage (V_{oc}), the short-circuit current (J_{sc}), and the fill factor (FF), are of great importance and should preferably be maximized to reach high PCEs. The open-circuit voltage is directly dependent on the positions of the energy levels of the highest occupied molecular orbital (HOMO) of the polymer and the lowest unoccupied molecular orbital (LUMO) of the acceptor.[8,9] To obtain a high J_{sc}, the mobility of charges and the nanoscale morphology of the active layer have been shown to be important parameters.[10−12]

*Corresponding author. Tel: +46 (0)31 772 34 01. Fax: +46 (0)31 772 34 18. E-mail: mats.andersson@chalmers.se.

(1) Hummelen, J. C.; Knight, B. W.; LePeq, F.; Wudl, F.; Yao, J.; Wilkins, C. L. *J. Org. Chem.* **1995**, *60*, 532–8.
(2) Reyes-Reyes, M.; Kim, K.; Carroll, D. L. *Appl. Phys. Lett.* **2005**, *87*, 083506/1–083506/3.
(3) Ma, W.; Yang, C.; Gong, X.; Lee, K.; Heeger, A. J. *Adv. Funct. Mater.* **2005**, *15*, 1617–1622.
(4) Brabec, C. J. *Sol. Energy Mater. Sol. Cells* **2004**, *83*, 273–292.
(5) Peet, J.; Kim, J. Y.; Coates, N. E.; Ma, W. L.; Moses, D.; Heeger, A. J.; Bazan, G. C. *Nat. Mater.* **2007**, *6*, 497–500.
(6) Jørgensen, M.; Norrman, K.; Krebs, F. C. *Sol. Energy Mater. Sol. Cells* **2008**, *92*, 686–714.
(7) Hauch, J. A.; Schilinsky, P.; Choulis, S. A.; Childers, R.; Biele, M.; Brabec, C. J. *Sol. Energy Mater. Sol. Cells* **2008**, *92*, 727–731.
(8) Brabec, C. J.; Cravino, A.; Meissner, D.; Sariciftci, N. S.; Fromherz, T.; Rispens, M. T.; Sanchez, L.; Hummelen, J. C. *Adv. Funct. Mater.* **2001**, *11*, 374–380.
(9) Scharber, M. C.; Muehlbacher, D.; Koppe, M.; Denk, P.; Waldauf, C.; Heeger, A. J.; Brabec, C. J. *Adv. Mater.* (*Weinheim, Germany*) **2006**, *18*, 789–794.
(10) Van Duren, J. K. J.; Yang, X.; Loos, J.; Bulle-Lieuwma, C. W. T.; Sieval, A. B.; Hummelen, J. C.; Janssen, R. A. J. *Adv. Funct. Mater.* **2004**, *14*, 425–434.
(11) Hoppe, H.; Niggemann, M.; Winder, C.; Kraut, J.; Hiesgen, R.; Hinsch, A.; Meissner, D.; Sariciftci, N. S. *Adv. Funct. Mater.* **2004**, *14*, 1005–1011.
(12) Zhang, F.; Jespersen, K. G.; Bjoerstroem, C.; Svensson, M.; Andersson, M. R.; Sundstroem, V.; Magnusson, K.; Moons, E.; Yartsev, A.; Inganaes, O. *Adv. Funct. Mater.* **2006**, *16*, 667–674.

Published on Web 07/09/2009

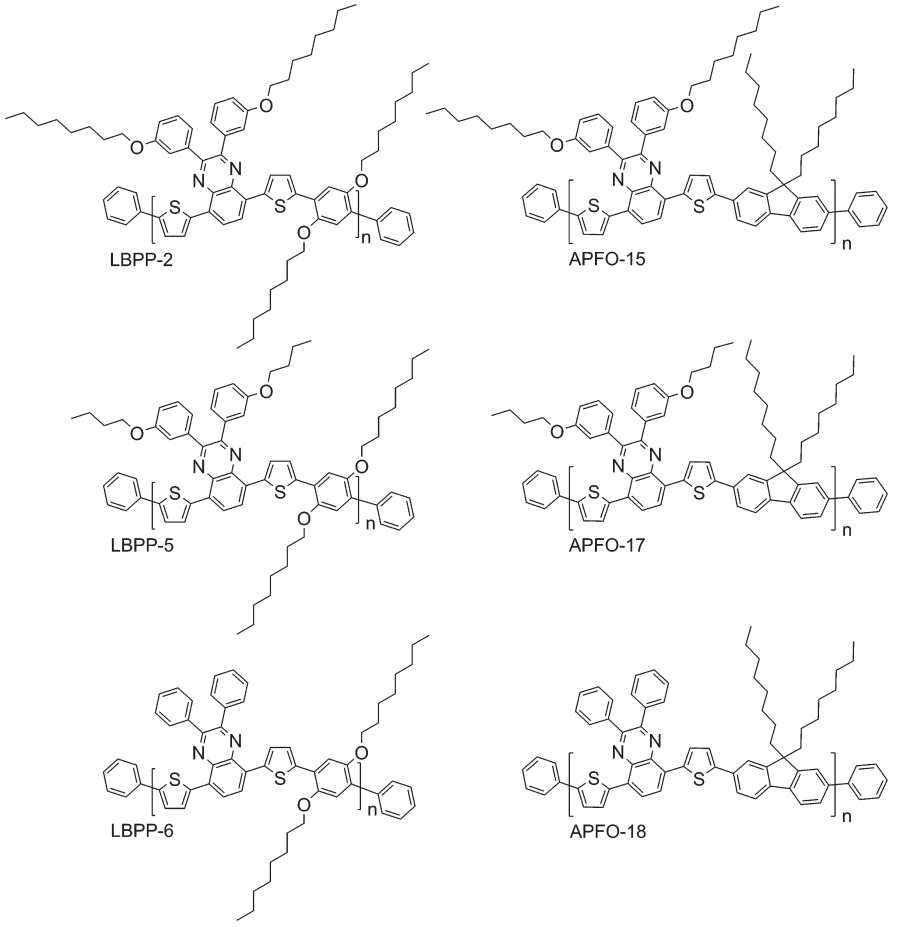

Figure 1. Polymer structures.

Low-band-gap polymers, synthesized with the objective to harvest photons of longer wavelengths, have emerged as promising materials for polymer solar cells.[13−15] The band gap can be controlled and reduced by incorporating alternating electron-donating (D) and electron-accepting (A) groups along the polymer backbone. This design induces an internal charge transfer (ICT) and results in a low band gap.[16] However, reducing the band gap must be done either by lowering the LUMO or raising the HOMO of the polymer. A low LUMO level could result in a reduced driving force for charge separation, that is, the energy difference between the LUMO levels of polymer and acceptor. It has been proposed that this energy difference should be at least 0.3 eV.[17] On the other hand, raising the HOMO level could result in a lower V_{oc}. Consequently, it is of great importance to match the energy levels of the polymer and acceptor carefully.

With the objective to gain further understanding of structure−property relationships of conjugated polymers for solar cells, a series of new polymers (Figure 1) based on the DAD approach has been synthesized. Inspired by the promising material APFO-15,[18] we synthesized a polymer with the same low-band-gap monomer but replaced the fluorene by a dialkoxy-phenylene monomer, resulting in the polymer LBPP-2. To extend the study further and investigate the influence of differences in substitution, we have prepared four additional polymers, two LBPPs and two APFOs, based on the structures of LBPP-2 and APFO-15. The polymers were obtained via Suzuki polycondensation reactions between 5,8-bis-(5-bromothiophen-2-yl)-2,3-diphenylquinoxaline monomers (with or without alkoxy substitution in the meta position of the phenyl rings) together with either 2,2′-(9,9-dioctyl-fluorene-2,7-diyl)bis(4,4,5,5-tetramethyl-1,3,2-dioxaborolane) or 2,2′-(2,5-bis(octyloxy)-1,4-phenylene)bis(4,4,5,5-tetramethyl-1,3,2-dioxaborolane). The resulting six polymers hence show structural differences at two points: (1) the length of the substituents on the low-band-gap monomers and/or (2) the comonomer, being either a fluorene or a phenylene derivative. The fluorene-based polymers are named APFO-15, 17, and 18, with octyloxy, butoxy, and no substitution on the low-band-gap monomers, respectively. The corresponding phenylene-based polymers are LBPP-2, 5, and 6.

(13) Winder, C.; Sariciftci, N. S. *J. Mater. Chem.* **2004**, *14*, 1077–1086.
(14) Bundgaard, E.; Krebs, F. C. *Solar Energy Mater. Sol. Cells* **2007**, *91*, 954–985.
(15) Kroon, R.; Lenes, M.; Hummelen, J. C.; Blom, P. W. M.; de Boer, B.; Taylor & Francis: 2008; Vol. *48*, pp 531−582.
(16) van Mullekom, H. A. M.; Vekemans, J. A. J. M.; Havinga, E. E.; Meijer, E. W. *Mater. Sci. Eng., R: Reports* **2001**, *R32*, 1–40.
(17) Bredas, J.-L.; Beljonne, D.; Coropceanu, V.; Cornil, J. *Chem. Rev.* **2004**, *104*, 4971–5003.
(18) Mammo, W.; Admassie, S.; Gadisa, A.; Zhang, F.; Inganaes, O.; Andersson, M. R. *Sol. Energy Mater. Sol. Cells* **2007**, *91*, 1010–1018.

The correlation between AFM images, solar-cell performances, and FET mobilities show that for these two groups of polymers, with similar molecular weight, optical absorption, and redox behavior, substituents play an important role in phase separation and mobility, which in turn has a great impact on device performance.

Experimental Section

General Details. All chemicals were purchased from Aldrich and used without further purification. The following compounds were synthesized using modified literature procedures: 4,7-bis(5-bromothiophen-2-yl)benzo[*c*][1,2,5]thiadiazole (**V**),[19] 5,8-bis(5-bromothiophen-2-yl)-2,3-bis(3-octyloxyphenyl)-quinoxaline (**VI**),[18] 2,2′-(2,5-bis(octyloxy)-1,4-phenylene)bis(4,4,5,5-tetramethyl-1,3,2-dioxaborolane) (**IX**),[20] and 2,2′-(9,9-dioctylfluorene-2,7-diyl)bis(4,4,5,5-tetramethyl-1,3,2-dioxaborolane) (**X**).[21] ^{1}H and ^{13}C NMR spectra were recorded at ambient temperature on a Varian VXR-300S spectrometer and a Varian UNITY-400 spectrometer. Chemical shifts are reported for solutions in $CDCl_3$ where residual $CHCl_3$ (δ_H 7.26 ppm, δ_C 77.16 ppm) is used as internal standard. Size-exclusion chromatography (SEC) was performed at 135 °C on a Waters Alliance 2000 GPCV, using RI detection and 1,2,4-trichlorobenzene as eluent at 1 mL/min. The SEC system was calibrated using polystyrene standards. UV−vis absorption spectroscopy of thin polymer films on glass substrates was performed on Perkin-Elmer UV/vis Lambda 20 spectrometer.

Square-Wave Voltammetry. SWV measurements were carried out on a CH-Instruments 650A Electrochemical Workstation. A three-electrode setup was used, with platinum wires both as working electrode and counter electrode, and Ag/Ag^+ was used as reference electrode. A 0.1 M solution of tetrabutylammonium hexafluorophosphate (Bu_4NPF_6) in anhydrous acetonitrile was used as supporting electrolyte. The polymers and fullerenes were deposited (together with a small amount of the Bu_4NPF_6) onto the working electrode from chloroform solutions. To remove oxygen from the electrolyte, the system was bubbled with nitrogen prior to each experiment. The nitrogen inlet was then moved to above the liquid surface and left there during the scans. The system was calibrated by measuring the potential, E^0, of the redox couple ferrocene/ferrocenium vs Ag/Ag^+.

Device Fabrication. The photovoltaic devices were fabricated by spin coating. As a buffer layer, the conductive polymer PEDOT-PSS (Baytron P VP Al 4083) was spin coated onto ITO-coated glass substrates, followed by annealing at 120 °C for 5 min to remove water. The active layers of mixed polymers and PCBMs ([60]PCBM or [70]PCBM) were spin coated from chloroform solutions onto the PEDOT-PSS layer. LiF (0.6 nm) and Al (60 nm) as the top electrode were deposited in vacuum onto the active layer. The thickness of the active layer was measured by a surface profiler, Dektak 6M. The size of the diode was defined by a mask when depositing Al in vacuum and was approximately 5 mm^2.

The external quantum efficiencies (EQEs) were calculated from the photocurrents at short-circuit conditions. The currents were recorded by a Keithley 485 picoammeter under illumination of monochromatic light through the ITO side of the devices. Current−voltage characteristics were recorded using a Keithley 2400 Source Meter under illumination of AM 1.5. The intensity of the light was 100 mW/cm^2 from a solar simulator (Model SS-50A, Photo Emission Tech., Inc.). All fabrications and characterizations were performed in ambient environment.

Atomic Force Microscopy. The surface morphology of the active layer was imaged by atomic force microscopy (AFM), using a Dimension 3100 system (Digital Instruments/Veeco) operating in tapping mode. Silicon cantilevers (NSG10) with a force constant of 5.5−22.5 N/m, a resonance frequency of 190−325 kHz, and a tip curvature radius of 10 nm were used.

Field-Effect Transistors (FETs). FETs were made from thermally oxidized highly doped p-type silicon wafers with an oxide thickness of 100 nm. Gold electrodes, with a chromium buffer layer, were thermally evaporated and patterned by lithography. Channel lengths (L) were in the range 10 and 50 μm and widths (W) around 5 mm. The active layer was spin coated on top. Evaluation of the FET data was made in the saturated regime from derivative plots of the square root of the source−drain current versus gate voltage. Where hysteresis or other effects prevents a constant slope, the maximum slope for outgoing (off to on) sweeps was used. Measurements were done under high vacuum ($\sim 10^{-6}$ torr).

Preparation of 3-Butoxybenzaldehyde (II). Potassium carbonate, K_2CO_3, (85.0 g, 615 mmol) was suspended in a solution of 3-hydroxybenzaldehyde (**I**) (15.0 g, 123 mmol) in dimethylformamide (DMF, 150 mL), and the mixture was heated to 100 °C under nitrogen atmosphere. 1-Bromobutane (34.0 g, 248 mmol) was added dropwise, and the reaction mixture was stirred at 100 °C under nitrogen overnight. After cooling to room temperature, the solid material was filtered off and water was added to the solution, which was extracted three times with diethyl ether. The combined ether extract was washed with 2 M HCl, 1 M NaOH, and water before drying over $MgSO_4$. Rotary evaporation of the solvent and excess bromobutane gave **II** (16.6 g, 0.093 mol, 76%) as a yellowish oil. ^{1}H NMR (300 MHz, $CDCl_3$, δ): 9.94 (s, 1H; CHO), 7.38−7.43 (m, 2H; Ar H), 7.36 (s, 1H; Ar H), 7.14 (m, 1H; Ar H), 3.99 (t, $J = 7$ Hz, 2H; CH_2), 1.75 (m, 2H; CH_2), 1.47 (m, 2H; CH_2), 0.96 (t, $J = 7$ Hz, 3H; CH_3).

Preparation of 1,2-Bis(3-butoxyphenyl)-2-hydroxyethanone (III). A solution of **II** (16.6 g, 93 mmol) and KCN (1.92 g, 29 mmol) in dimethylformamide (DMF, 40 mL) was stirred at 80 °C under nitrogen atmosphere for 36 h after which water (40 mL) was added. The aqueous solution was extracted three times with diethyl ether, and the combined extract was washed with 2 M HCl and water, dried over $MgSO_4$, and concentrated by rotary evaporation. The crude product was further purified by column chromatography on silica gel (hexane/toluene/methanol, 10:1:1, as eluent) yielding **III** (11.0 g, 30.9 mmol, 66%). ^{1}H NMR (300 MHz, $CDCl_3$, δ): 7.46 (m, 2H; Ar H), 7.14−7.26 (m, 3H; Ar H), 7.05 (d, $J = 8$ Hz, 1H; Ar H), 6.84 (s, 1H; Ar H), 6.80 (d, $J = 8$ Hz, 1H; Ar H), 5.88 (s, 1H; CH), 3.95 (m, 4H; CH_2), 1.74 (m, 4H; CH_2), 1.45 (m, 4H; CH_2), 0.97 (t, $J =$ 7 Hz, 6H; CH_3).

Preparation of 1,2-Bis(3-butoxyphenyl)ethane-1,2-dione (IV). To a solution of **III** (11.0 g, 30.9 mmol) in dimethyl sulfoxide (DMSO, 40 mL), HBr (48 wt % in water, 17 mL, 150 mmol) was added dropwise during 45 min. The solution was stirred at 50 °C for 4 h followed by stirring at 90 °C overnight and was then poured onto ice water whereupon a brown solid material precipitated. The precipitate was dissolved in ethyl acetate, and the aqueous phase was further extracted twice with ethyl acetate. The organic extracts were combined, washed with water, and dried over magnesium sulfate. Evaporation of the

(19) Svensson, M.; Zhang, F.; Veenstra, S. C.; Verhees, W. J. H.; Hummelen, J. C.; Kroon, J. M.; Inganaes, O.; Andersson, M. R. *Adva. Mater.* (*Weinheim, Germany*) **2003**, *15*, 988–991.
(20) Aubert, P.-H.; Knipper, M.; Groenendaal, L.; Lutsen, L.; Manca, J.; Vanderzande, D. *Macromolecules* **2004**, *37*, 4087–4098.
(21) Ranger, M.; Rondeau, D.; Leclerc, M. *Macromolecules* **1997**, *30*, 7686–7691.

solvent followed by recrystallization from ethanol/water gave **IV** (6.2 g, 17.5 mmol, 57%) as pale-yellow crystals. ^{1}H NMR (300 MHz, $CDCl_3$, δ): 7.51 (s, 2H; Ar H), 7.45 (d, $J = 8$ Hz, 2H; Ar H), 7.38 (t, $J = 8$ Hz, 2H; Ar H), 7.19 (d, $J = 8$ Hz, 2H; Ar H), 4.02 (t, $J = 7$ Hz, 4H; CH_2), 1.78 (m, 4H; CH_2), 1.50 (m, 4H; CH_2), 0.98 (t, $J = 7$ Hz, 6H; CH_3). ^{13}C NMR (75 MHz, $CDCl_3$, δ): 194.5 (C=O), 159.6 (C-3), 134.2 (C-1), 130.0 (C-5), 122.9 (C-6), 122.2 (C-4), 113.6 (C-2), 68.0 (C-1′), 31.1 (C-2′), 19.2 (C-3′), 13.8 (C-4′).

Preparation of 5,8-Bis(5-bromothiophen-2-yl)-2,3-bis(3-butoxyphenyl)quinoxaline (VII). To a solution of 4,7-bis(5-bromothiophen-2-yl)benzo[1,2,5]thiadiazole (**V**) (590 mg, 1.29 mmol) in acetic acid (20 mL) was added zinc dust (1.0 g, 16 mmol), and the mixture was stirred at 80 °C. After 2 h of reaction, thin-layer chromatography (silica gel, chloroform as eluent) suggested complete consumption of **V**, and the mixture was filtered. The solution was basified with 2 M NaOH and extracted three times with dichloromethane. The solvent from the combined organic extracts was removed on a rotary evaporator, the resulting orange solid was dissolved in acetic acid (20 mL), and the dione **IV** (300 mg, 846 mmol) was added to the solution. The solution was stirred at 60 °C overnight, whereupon orange crystals precipitated. The solid material was filtered off and washed with water. Column chromatography on silica gel (petroleum ether/dichloromethane, 2:1, as eluent) gave **VII** (381 mg, 509 mmol, 60%) as orange crystals. ^{1}H NMR (300 MHz, $CDCl_3$, δ): 8.07 (s, 2H; Ar H), 7.55 (d, $J = 4$ Hz, 2H; Th H), 7.54 (s, 2H; Ar H), 7.22 (t, $J = 8$ Hz, 2H; Ar H), 7.12 (d, $J = 4$ Hz, 2H; Th H), 7.11 (d, $J = 8$ Hz, 2H; Ar H), 6.98 (d, $J = 8$ Hz, 2H; Ar H), 4.06 (t, $J = 7$ Hz, 4H; CH_2), 1.79 (m, 4H; CH_2), 1.52 (m, 4H; CH_2), 0.99 (t, $J = 7$ Hz, 6H; CH_3). ^{13}C NMR (100 MHz, $CDCl_3$, δ): 159.5 (C-3″), 155.2 (C-2, C-3), 152.0 (C-9, C-10), 139.5 (C-2′), 136.5 (C-1″), 130.6 (C-5, C-8), 129.3 (C-4′), 129.2 (C-3′), 125.7 (C-5″), 125.6 (C-6, C-7), 123.1 (C-6″), 117.4 (C-5′), 115.4 (C-4″), 115.3 (C-2‴), 68.2 (C-1‴), 31.6 (C-2‴), 19.6 (C-3‴), 14.2 (C-4‴).

Preparation of 5,8-Bis(5-bromothiophen-2-yl)-2,3-diphenylquinoxaline (VIII). Compound **V** (891 mg, 1.95 mmol) was dissolved in acetic acid (25 mL), and zinc dust (1.53 g, 23.4 mmol) was added to the solution. The mixture was stirred at 80 °C and followed by TLC (silica gel, chloroform as eluent). After 3 h the reaction mixture was filtered, and the residue was washed with acetic acid (15 mL). Benzil (867 mg, 4.12 mmol) was added to the filtrate, and the mixture was stirred at 60 °C for 1 h and at room temperature overnight. The orange precipitate was filtered off and washed with acetic acid and water. Column chromatography on silica gel (petroleum ether/toluene, 1:1 as eluent) gave **VI** (270 mg, 447 mmol, 23%) as an orange crystalline material. ^{1}H NMR (400 MHz, $CDCl_3$, δ): 8.06 (s, 2H; Ar H), 7.69 (d, $J = 7$ Hz, 4H; Ar H), 7.56 (d, $J = 4$ Hz, 2H; Th H), 7.38−7.45 (m, 6H; Ar H), 7.12 (d, $J = 4$ Hz, 2H; Th H). ^{13}C NMR (100 MHz, $CDCl_3$, δ): 155.2 (C-2, C-3), 152.4 (C-9, C-10), 138.4 (C-2′), 136.9 (C-1″), 130.7 (C-5, C-8), 129.4 (C-4′), 129.3 (C-3′), 128.5 (C-3″), 128.4 (C-4″), 126.0 (C-2″), 125.8 (C-6, C-7), 117.4 (C-5′). ^{13}C NMR (100 MHz, $CDCl_3$, δ): 155.2 (C-2, C-3), 152.4 (C-9, C-10), 138.4 (C-2′), 136.9 (C-1″), 130.8 (C-5, C-8), 130.7 (C-3′), 129.3 (C-4′), 129.2 (C-5″), 125.7 (C-3′), 125.6 (C-6, C-7), 123.1 (C-6″), 117.4 (C-4″), 117.2 (C-2″).

Preparation of LBPP-2 (General Procedure for Polymerization). The monomers, **VI** (70.0 mg, 0.119 mmol) and **IX** (102.7 mg, 0.119 mmol), were dissolved in degassed toluene (10 mL), and tetrakis(triphenylphosphine)Pd^0 (14 mg, 0.012 mmol) was added to the solution. The mixture was heated to reflux for 10 min, after which degassed tetraethylammonium hydroxide solution (20 wt % in water, 0.45 mL, 0.64 mmol) was added using a syringe. The mixture was heated under reflux (nitrogen atmosphere) for 5 h. Phenylboronic acid (30 mg) was added to the solution and allowed to react for 1 h before bromobenzene (50 mg) was introduced. One hour after the addition of bromobenzene, the mixture was allowed to cool to room temperature, and the polymer was precipitated in methanol (200 mL) and was collected on a PTFE-membrane filter. The polymer was then dissolved in chloroform (50 mL), and the resulting solution was washed twice with ammonia (25 wt % in water, 20 mL) and twice with water (50 mL). After concentration by rotary evaporation, the polymer was reprecipitated in methanol, collected on a membrane filter, and transferred to an extraction thimble. To remove low-molecular weight oligomers, the crude material was Soxhlet extracted with diethyl ether for 3 h. After Soxhlet extraction with chloroform, the resulting chloroform solution was concentrated by rotary evaporation, and the polymer LBPP-2 was obtained as a dark powder (103.0 mg, 84%) after precipitation in methanol. ^{1}H NMR (400 MHz, $CDCl_3$, δ): 8.23 (s, 2H), 7.96 (br, 2H), 7.71 (br, 2H), 7.50 (s, 2H), 7.27−7.37 (br m, 6H), 6.96 (br d, 2H), 4.09 (br t, 4H), 3.88 (br t, 4H), 1.79 (br, 4H), 1.45−1.70 (br m, 12H), 1.10−1.35 (br, 32H), 0.81 (br t, 12H).

Preparation of LBPP-5. Following the general procedure, **VII** (mg, mmol) and **IX** (mg, mmol) were used. The polymer was obtained as a dark powder (149.6 mg, 91%). ^{1}H NMR (400 MHz, $CDCl_3$, δ): 8.22 (s, 2H), 7.97 (br, 2H;), 7.71 (br, 2H), 7.47 (s, 2H), 7.27−7.38 (br m, 6H), 6.96 (br d, 2H), 4.09 (br t, 4H), 3.88 (br t, 4H), 1.79 (br, 4H), 1.45−1.70 (br m, 12H), 1.15−1.40 (br, 16H), 0.78−0.90 (dt, 12H).

Preparation of LBPP-6. Following the general procedure, **VIII** (mg, mmol) and **IX** (mg, mmol) were used. The polymer was obtained as a dark powder (19.1 mg, 14%). Because of precipitation of solid material in the polymerization mixture, phenylboronic acid and bromobenzene were added after 2.75 and 3.75 h, respectively. The low yield is caused by the large fraction of chloroform-insoluble material left in the extraction thimble after Soxhlet extraction. ^{1}H NMR (400 MHz, $CDCl_3$, δ): 8.21 (br, 2H), 7.97 (br, 2H;), 7.70−7.81 (br m, 6H), 7.34−7.46 (br m, 8H), 4.13 (br t, 4H), 1.85 (br, 4H), 1.52 (br, 4H), 1.15−1.43 (br, 16H), 0.84 (t, 6H).

Preparation of APFO-15. Following the general procedure, **VI** (mg, mmol) and **X** (mg, mmol) were used. The polymer was obtained as a dark-red colored powder (116.9 mg, 92%). ^{1}H NMR (400 MHz, $CDCl_3$, δ): 8.23 (s, 2H), 7.97 (br, 2H), 7.74 (br, 4H), 7.70 (br, 2H), 7.50 (br, 2H), 7.46 (d, 2H), 7.40 (s, 2H), 7.35 (t, 2H), 7.00 (br d, 2H), 3.90 (br t, 4H), 2.10 (br, 4H), 1.71 (br, 4H), 1.15−1.45 (br m, 44H), 0.86 (t, 6H), 0.78 (t, 6H).

Preparation of APFO-17. Following the general procedure, **VII** (mg, mmol) and **X** (mg, mmol) were used. The polymer was obtained as a dark-red colored powder (157.8 mg, 94%). ^{1}H NMR (400 MHz, $CDCl_3$, δ): 8.22 (s, 2H), 7.96 (br, 2H), 7.74 (br, 4H), 7.70 (br, 2H), 7.50 (br, 2H), 7.45 (d, 2H), 7.42 (s, 2H), 7.35 (t, 2H), 7.00 (br d, 2H), 3.92 (br t, 4H), 2.09 (br, 4H), 1.70 (m, 4H), 1.41 (m, 4H), 1.05−1.25 (br m, 24H), 0.92 (t, 6H), 0.78 (t, 6H).

Preparation of APFO-18. Following the general procedure, **VIII** (mg, mmol) and **X** (mg, mmol) were used. The polymer was obtained as a dark-red colored powder (72.0 mg, 51%). Because of some precipitation of solid material in the polymerization mixture, phenylboronic acid and bromobenzene were added after 4.25 and 5.25 h, respectively. The moderate yield is caused by the substantial fraction of chloroform-insoluble material left in the extraction thimble after Soxhlet extraction. ^{1}H

Scheme 1. Synthesis of the Monomers VII and VIII

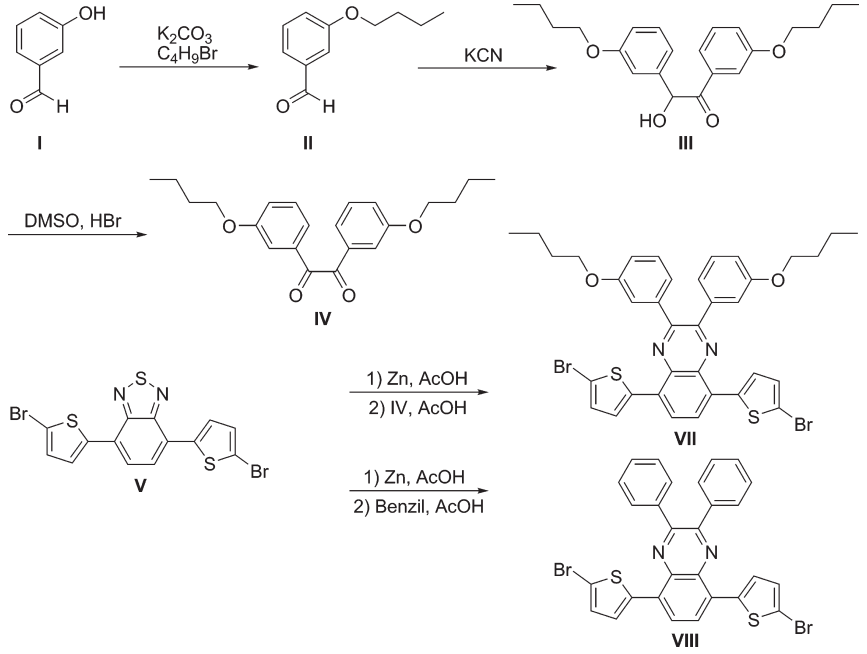

Scheme 2. Suzuki Polycondensation Reaction of the Low-Band-Gap Monomers Together with Diboronic Esters of Fluorene or Phenylene

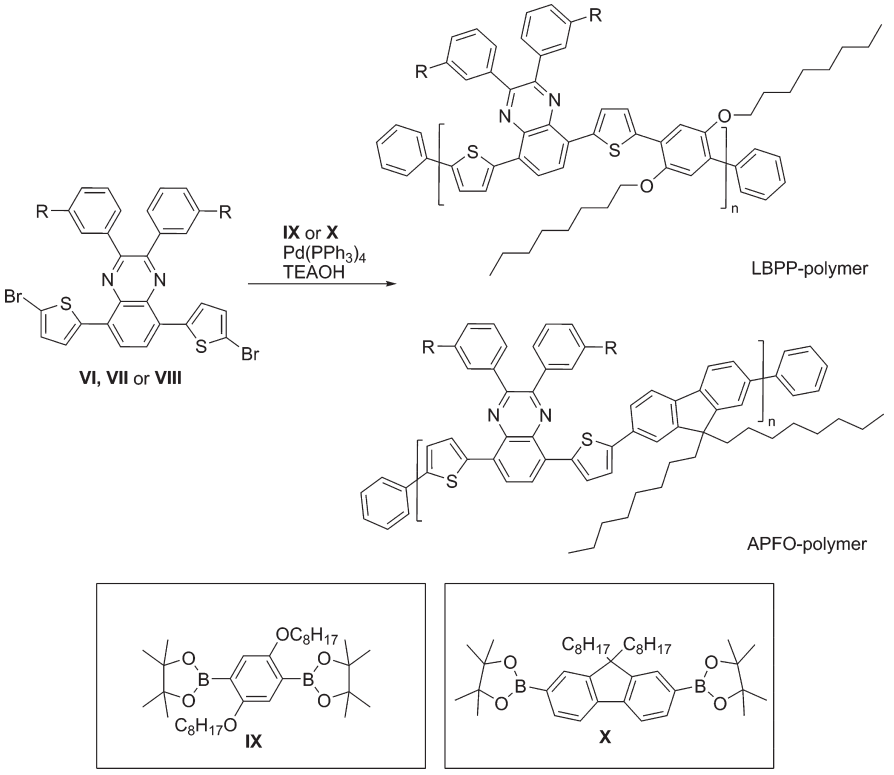

NMR (400 MHz, $CDCl_3$, δ): 8.22 (s, 2H), 7.94 (br, 2H), 7.88 (br, 2H), 7.68−7.78 (br m, 6H), 7.42−7.52 (br m, 10H), 2.10 (br, 4H), 1.02−1.23 (br m, 24H), 0.76 (t, 6H).

Results and Discussion

Polymer Synthesis and Characterization. The synthetic route to the DAD monomers **VII** and **VIII** is outlined in Scheme 1, and a summary of the six polymerization reactions is presented in Scheme 2. Monomer **VI** was synthesized according to a previously published procedure.[22] However, following the same procedure to synthesize the new monomer, **VII**, resulted in unexpected purification problems. Thus, a different synthetic route was chosen, as outlined in Scheme 1. After alkylation of the hydroxyaldehyde **I**, the resulting butoxyaldehyde was

(22) Gadisa, A.; Mammo, W.; Andersson, L. M.; Admassie, S.; Zhang, F.; Andersson, M. R.; Inganaes, O. *Adv. Funct. Mater.* **2007**, *17*, 3836–3842.

Table 1. Polymerization Yields Calculated from the Chloroform-Soluble Fraction Together with Molecular Weights and Polydispersity Indices Determined by SEC Using Polystyrene Standards

		molecular weight		
polymer	yield (%)	M_n	M_w	PDI
APFO-15	92	15 300	36 400	2.4
APFO-17	94	13 300	30 600	2.3
APFO-18	51	8 400	18 800	2.2
LBPP-2	84	13 300	27 900	2.1
LBPP-5	91	12 000	26 000	2.2
LBPP-6	14	3 600	5 800	1.6

treated with KCN in DMF.[23] The condensation product was further oxidized with DMSO/HBr to afford compound **IV**. Monomers **VII** and **VIII** were synthesized by condensation of the diamine, obtained after reduction of 4,7-bis(5-bromothiophene-2-yl)benzo[1,2,5]thiadiazole, **V**, with the diones **IV** and benzil, respectively.

All three low-band-gap monomers were copolymerized together with both 2,2′-(2,5-bis(octyloxy)-1,4-phenylene)-bis(4,4,5,5-tetramethyl-1,3,2-dioxaborolane),[20] **IX**, and 2,2′-(9,9-dioctylfluorene-2,7-diyl)bis(4,4,5,5-tetramethyl-1,3,2-dioxaborolane),[21] **X**, resulting in three phenylene-type polymers (LBPP polymers) and three fluorene-type polymers (APFO polymers). The Suzuki cross-coupling reaction was employed for the polymerization reactions, and phenylboronic acid and bromobenzene were added after the polymerization time as end-capping agents. The polymers were obtained using nearly identical reaction conditions (0.023−0.024 M total monomer concentration, equimolar amounts of monomers, 5.1−5.2 mol % catalyst, refluxing toluene, and nitrogen atmosphere), and reaction times were 5.25 h except for when **VIII** was employed. Both polymerization reactions involving **VIII**, which led to LBPP-6 and APFO-18, were stopped earlier because of precipitation of solid material in the reaction mixtures, which is why end-capping instead was started already after 2.75 and 4.25 h, respectively. The reason for this behavior with monomer **VIII** can be explained by the absence of solubilizing groups, resulting in low solubility of the formed high-molecular-weight polymer. After end-capping, precipitation, and washing with ammonia and water, the polymeric materials were extracted with diethyl ether to remove low molecular-weight oligomers, and the final products were obtained by extraction with chloroform. Table 1 shows polymerization yields, calculated based on the chloroform-soluble fractions of the polymers. The yields of LBPP-6 and APFO-18 were poorer because of the low solubility of these materials, as evidenced by insoluble material left in the extraction thimbles after chloroform extraction.

Molecular-weight distributions of the polymers were obtained using size-exclusion chromatography (SEC), as described in the Experimental Section. Number-averaged (M_n) and weight-averaged (M_w) molecular weights were determined using a polystyrene-standard calibration, and the results are presented in Table 1. The SEC measurements revealed that the APFO polymers have slightly higher molecular weights compared to their LBPP analogues. Furthermore, molecular weights decrease as the length of the solubilizing groups on the low-band-gap monomers are shortened from octyloxy to butoxy. The chloroform-soluble fractions of the polymers containing **VIII**, that is, LBPP-6 and APFO-18, were obtained in relatively low molecular weights, a result that once again can be attributed to the absence of solubilizing groups on the low-band-gap monomer.

(23) Koehler, H.; Kempe, U.; Dockner, T.; Saukel, H.. Patent Application: DE, **1988**; p 3 (BASF A.-G., Fed. Rep. Ger.).

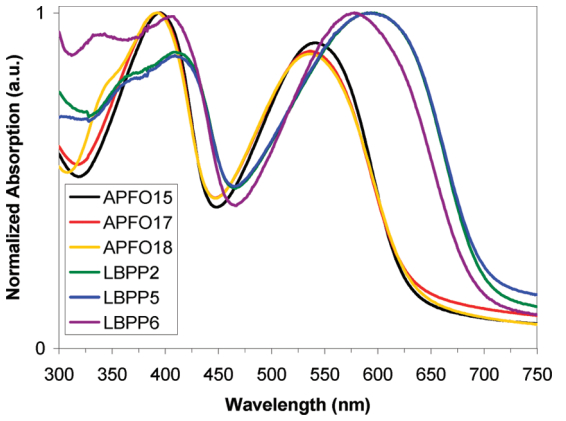

Figure 2. Optical absorption of polymer films spin coated onto glass substrates.

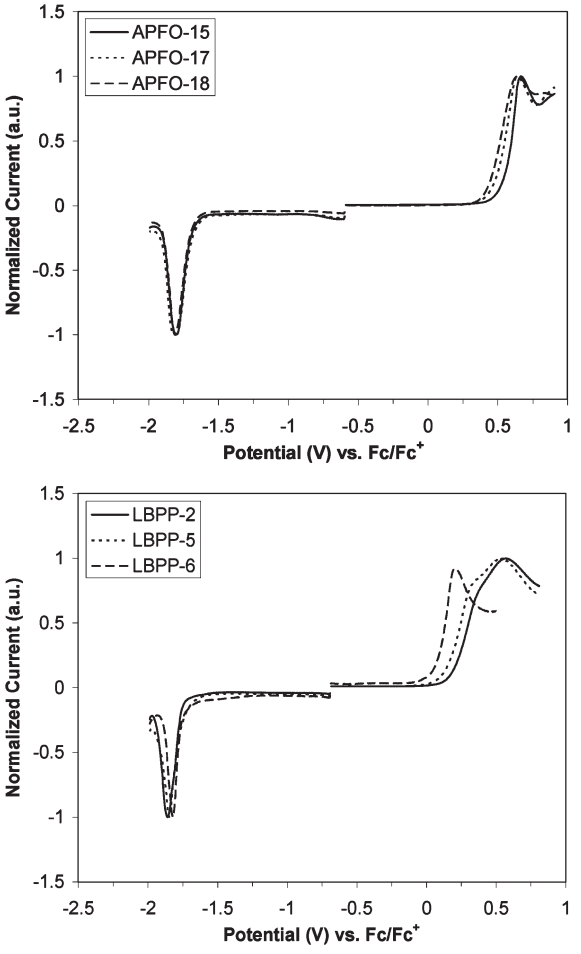

Figure 3. Square-wave voltammograms showing the redox behavior (third cycle) of the APFO polymers (top) and the LBPP polymers (bottom).

Absorption spectra of polymer films, spin coated onto glass substrates, are shown in Figure 2. The spectra

Table 2. Data from Square-Wave Voltammetry (SWV) Together with Estimated HOMO and LUMO Levels from Both Onset and Peak Potentials

	SWV: onset potentials					SWV: peak potentials				
	E^{ox} (V)[a]	E^{red} (V)[b]	HOMO (eV)[c]	LUMO (eV)[c]	E_g^{ec} (eV)[d]	E^{ox} (V)[a]	E^{red} (V)[b]	HOMO (eV)[c]	LUMO (eV)d	E_g^{ec} (eV)[d]
APFO-15	0.56	−1.70	−5.69	−3.43	2.3	0.67	−1.80	−5.80	−3.33	2.5
APFO-17	0.48	−1.69	−5.61	−3.44	2.2	0.64	−1.80	−5.77	−3.33	2.4
APFO-18	0.43	−1.70	−5.56	−3.43	2.1	0.64	−1.80	−5.77	−3.33	2.4
LBPP-2	0.19	−1.76	−5.32	−3.37	2.0	0.36*	−1.86	−5.49	−3.27	2.2
LBPP-5	0.15	−1.76	−5.28	−3.37	1.9	0.34*	−1.85	−5.47	−3.28	2.2
LBPP-6	0.09	−1.76	−5.22	−3.37	1.9	0.21	−1.82	−5.34	−3.31	2.0
[60]PCBM	1.42	−0.94	−6.55	−4.19	2.4	1.47	−1.03	−6.60	−4.10	2.5
[70]PCBM	1.31	−0.88	−6.44	−4.25	2.2	1.38	−0.98	−6.51	−4.15	2.4

[a] Oxidation potential vs ferrocene. [b] Reduction potential vs ferrocene. [c] Estimated HOMO/LUMO energy levels from HOMO/LUMO = $-(E^{ox/red}+5.13)$ eV. [d] Electrochemical band gap.

clearly show that within the two series of polymers there are no major differences in optical absorption. However, there is a difference in absorption between the two series of polymers, which can be explained by the two different comonomers used. The dialkoxy-phenylene unit is more electron rich compared to a fluorene unit, a property that pronounces the electron-donating nature, and thereby emphasizes the donor−acceptor−donor character in the polymer backbone. Consequently, the LBPP polymers have a more pronounced internal-charge transfer (ICT) and exhibit a red-shifted absorption compared with their APFO analogues. For the APFO polymers, the onset of absorption is around 630 nm, corresponding to an optical band gap of 2.0 eV, and for the LBPP polymers the onset is higher, around 700 nm for LBPP-2 and 5 and slightly lower for LBPP-6, corresponding to an optical band gap of 1.8 eV. The fact that LBPP-6 has a somewhat blue-shifted absorption compared with the other LBPP polymers can be attributed to the relatively lower molecular weight of this polymer.

Electrochemical Properties. The positions of the highest occupied molecular orbital (HOMO) and the lowest unoccupied molecular orbital (LUMO) of the polymers are of great importance when using the materials in solar cells. These positions can be correlated to the oxidation and reduction potentials obtained in electrochemical measurements. The oxidation potential, that is, ionization potential (IP), is generally considered to be an estimate of the HOMO level. Furthermore, the reduction potential, that is, electron affinity (EA), corresponds to the LUMO position. The electrochemical band gap E_g^{ec} is defined as the difference between IP and EA. Traditionally, cyclic voltammetry (CV) has been used to determine the redox behavior of conjugated polymers. However, we found that square-wave voltammetry (SWV),[24] used earlier for similar materials,[18,25] was superior to CV, being more sensitive and resulting in much clearer peaks in the voltammograms. Hence, this method facilitates an easier estimation of the potentials for oxidation and reduction. Square-wave voltammograms showing the oxidative and reductive doping behavior of the polymers are shown in Figure 3. We have chosen to determine the ionization potentials and electron affinities both from the peak potentials (E_p^{ox} and E_p^{red}) and the onset potentials ($E^{ox}{}_{onset}$ and $E^{red}{}_{onset}$) in the voltammograms. The use of onsets instead of peaks is common for conjugated polymers, which can show rather complicated voltammograms, and has been proposed to be a more accurate method.[26] One advantage with this is if two or more peaks are unresolved, making it difficult to determine the peak potentials, for example, the oxidation peaks of LBPP-2 and LBPP-6 in Figure 3. The positions of the onsets are here defined as the intercept between the extended baseline and the maximum-derivative tangent. The energy levels and electrochemical band gaps, from both onset and peak potentials, are found in Table 2. The HOMOs and LUMOs were calculated by setting the oxidative peak potential, E_p^{ox}, of ferrocene/ferrocenium vs the normal-hydrogen electrode (NHE) to 0.630 V[27] and the NHE energy level relative to vacuum to 4.5 eV,[28] resulting in the general correlation HOMO/LUMO = $-(E^{ox/red}+5.13)$ eV.

The results from the SWV measurements of the polymers show that the electrochemical band gaps are slightly larger compared with the optical band gaps, which are 2.0 eV for the APFOs and 1.8 eV for the LBPPs. Regardless of which method is used, that is, peaks or onsets, it is clear that potentials for reduction are positioned within a relatively narrow potential range for both the APFOs and the LBPPs, resulting in LUMO levels of approximately −3.4 eV (from onsets) or −3.3 eV (from peaks). The greatest difference is seen when comparing the HOMO levels for the APFOs with the corresponding levels for LBPPs, where the LBPPs are shifted toward the vacuum level, which is agreement with results (lower V_{oc}) from photovoltaic cells presented in the next section.

The driving force for charge separation, i.e., the difference between the LUMO levels of polymer and acceptor, is an important property for polymer solar cells. To investigate this driving force in our polymer−acceptor series, square-wave voltammetry was performed as described above on both [60]PCBM and [70]PCBM with estimated HOMO and LUMO levels shown in Table 2. When comparing the LUMO levels of the acceptors and

(24) Osteryoung, J. G.; Osteryoung, R. A. Anal. Chem. **1985**, *57*, 101A−102A, 105A−106A, 108A, 110A.
(25) Admassie, S.; Inganaes, O.; Mammo, W.; Perzon, E.; Andersson, M. R. *Synth. Met.* **2006**, *156*, 614–623.
(26) Johansson, T.; Mammo, W.; Svensson, M.; Andersson, M. R.; Inganaes, O. *J. Mater. Chem.* **2003**, *13*, 1316–1323.
(27) Pavlishchuk, V. V.; Addison, A. W. *Inorg. Chim. Acta* **2000**, *298*, 97–102.
(28) Bard, A. J.; Faulkner, L. R. Electrochemical Methods: Fundamentals and Applications; Wiley: New York, 1980.

Table 3. Photovoltaic Properties of Devices Prepared from the Six Polymers

	[60]PCBM					[70]PCBM				
	spin speed (rpm)	J_{sc} (mA/cm^2)[a]	V_{oc} (V)[b]	FF[c]	PCE (%)[d]	spin speed (rpm)	J_{sc} (mA/cm^2)[a]	V_{oc} (V)[b]	FF[c]	PCE (%)[d]
APFO-15	1000	3.02	0.97	0.62	1.83	1000	2.09	0.98	0.54	1.10
	2000	3.73	0.97	0.60	2.17	4000	4.51	0.99	0.56	2.51
APFO-17	1000	3.72	0.94	0.50	1.75	1000	3.25	0.98	0.50	1.60
	2000	4.03	0.97	0.55	2.12	4000	5.21	0.99	0.57	2.90
APFO-18	1000	4.03	0.92	0.50	1.87	1000	4.34	0.97	0.54	2.26
	2000*	4.33*	0.94*	0.51*	2.06*	4000	5.25	0.97	0.57	2.90
LBPP-2	1500	4.68	0.77	0.56	2.01	2000	4.34	0.79	0.58	2.01
	2500	4.24	0.75	0.64	2.04	4000	4.70	0.79	0.66	2.47
LBPP-5	1500	4.56	0.69	0.48	1.50	2000	7.11	0.71	0.52	2.59
	2500	4.24	0.71	0.56	1.68	4000	6.54	0.71	0.60	2.82
LBPP-6	1500	1.46	0.50	0.48	0.35	2000	2.33	0.53	0.53	0.64
	2500	1.89	0.48	0.42	0.38	4000	3.84	0.52	0.51	1.01

[a] Short-circuit current (J_{sc}). [b] Open-circuit voltage (V_{oc}). [c] Fill factor (FF). [d] Power-conversion efficiency (PCE) for photovoltaic cells prepared from all polymers together with the acceptors [60]PCBM (left) and [70]PCBM (right). Furthermore, the cells were prepared using different spin speeds during spin coating. Data are obtained under illumination from AM1.5 (1000 Wm^{-2}) and presented as average values of three separate cells (except *, which is only one cell).

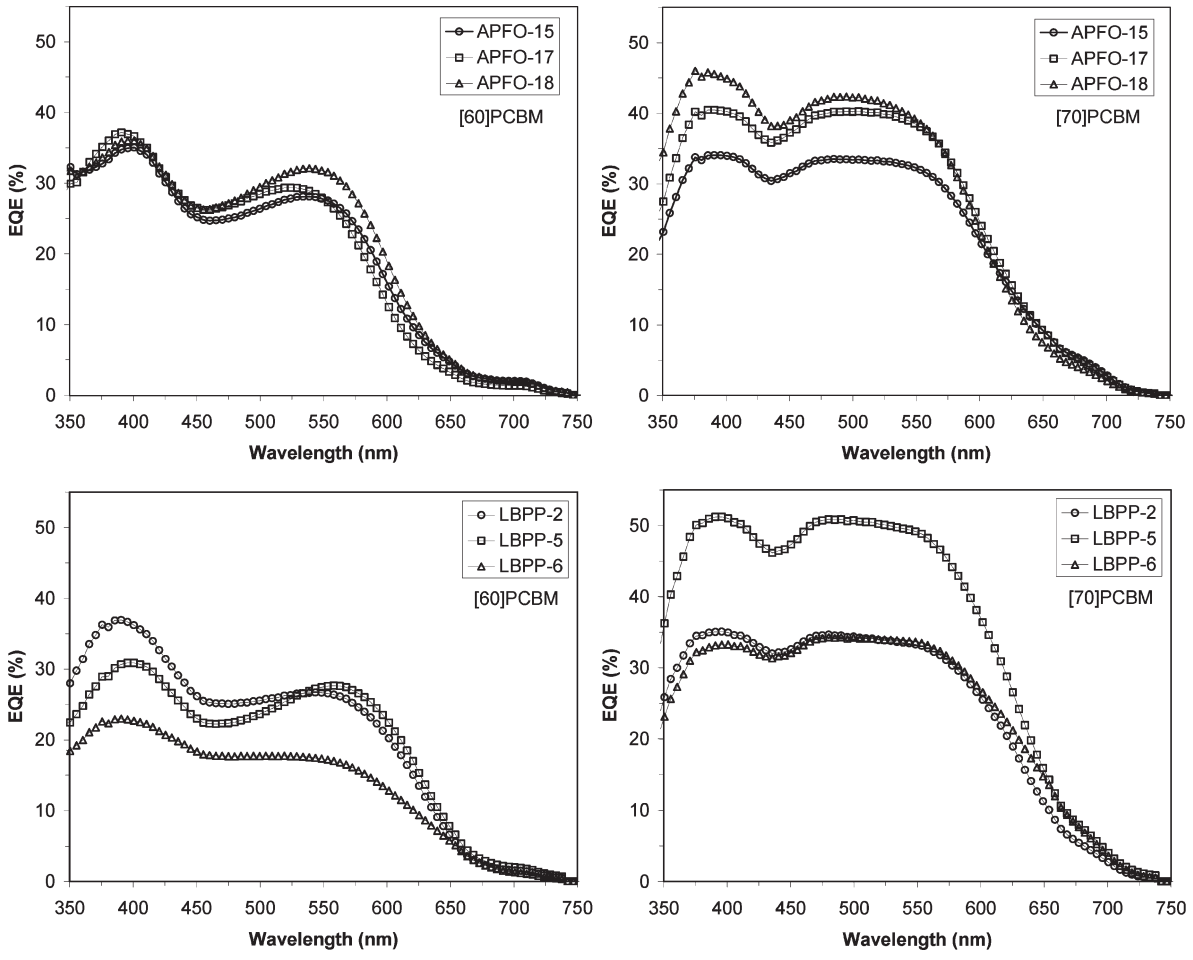

Figure 4. External quantum efficiencies of photovoltaic cells prepared from APFO polymers (top) and LBPP polymers (bottom) together with [60]PCBM (left) and [70]PCBM (right).

the polymers, it is seen that the energy differences are at least 0.8 eV for all polymer−acceptor mixtures, which is sufficient to result in an efficient charge transfer, that is, higher than the suggested 0.3 eV.[17]

Fabrication and Characterization of Photovoltaic Cells. A series of photovoltaic cells were prepared of all six polymers and both [60]PCBM and [70]PCBM as electron-accepting materials. The devices have the general structure ITO/PEDOT:PSS/polymer:fullerene/LiF/Al. After deposition of a PEDOT:PSS layer on top of the anode (ITO), the active material was deposited via spin coating from a chloroform solution of polymer and fullerene (1:4 by weight). To extend the study further and pronounce the influence of morphology and film thickness, all polymer:fullerene mixtures were spin coated on top of the PEDOT:PSS layer at two different spin speeds. For the

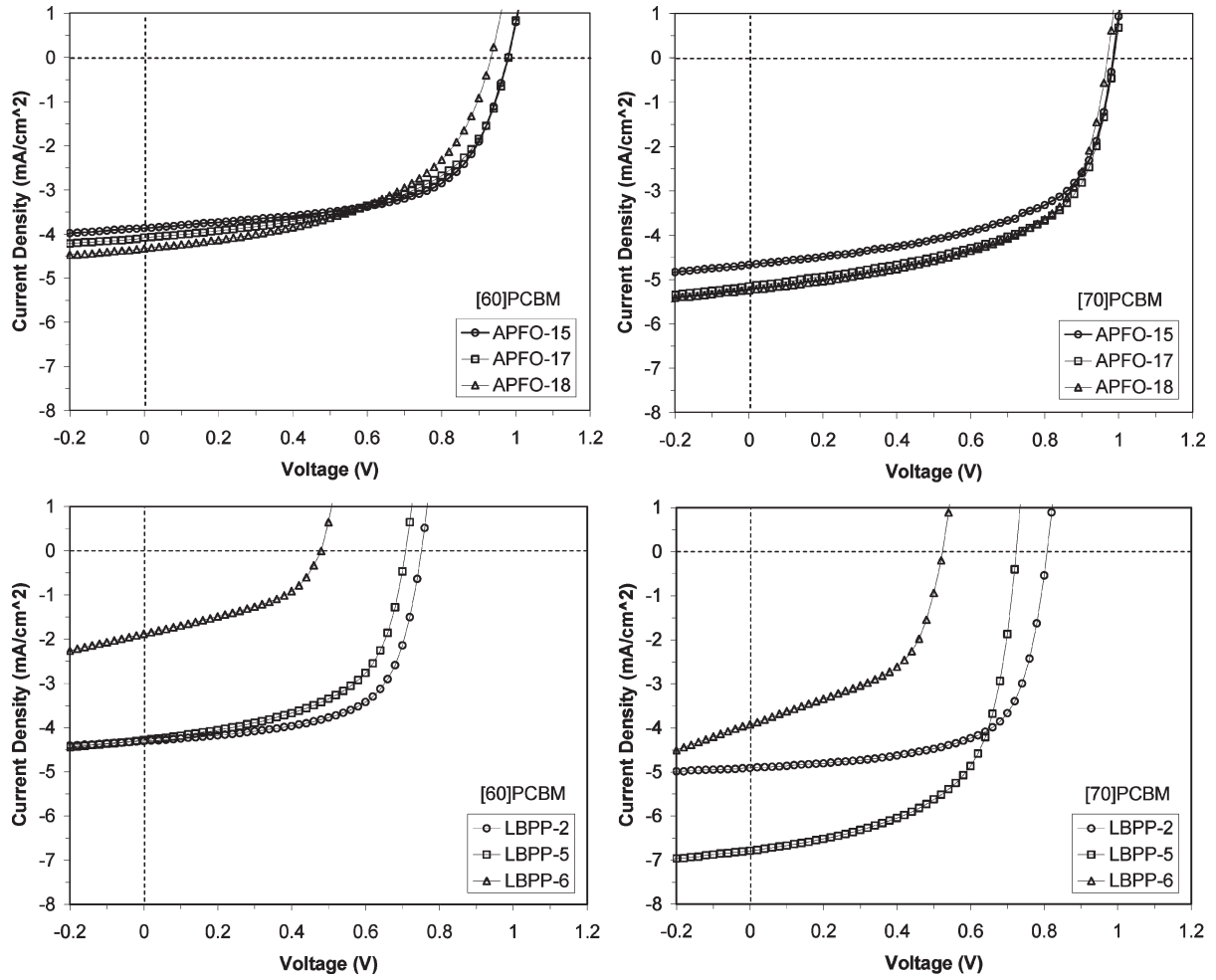

Figure 5. *I*−*V* characteristics of photovoltaic cells prepared from APFO polymers (top) and LBPP polymers (bottom) together with [60]PCBM (left) and [70]PCBM (right).

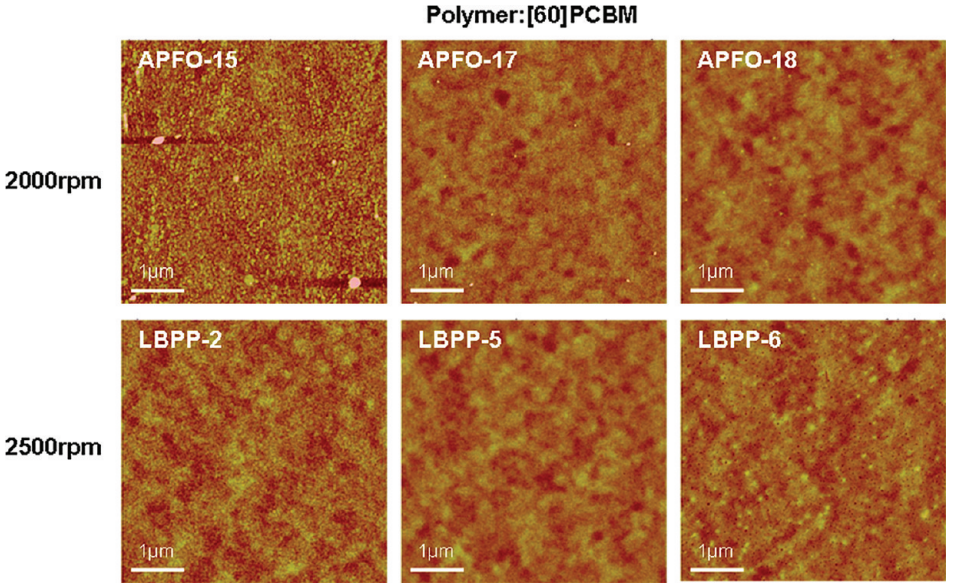

Figure 6. AFM images (height) of [60]PCBM:polymer mixtures (spin coated at high speeds), showing the morphology on a micrometer scale.

[60]PCBM devices the spin speeds used during spin coating were (presented as high/low speed) 1000/2000 rpm and 1500/2500 rpm for the APFO and LBPP polymers, respectively, and the corresponding speeds for the [70]PCBM analogues were 1000/4000 rpm and 2000/4000 rpm. Using different spin speeds has an influence on the thickness of the active polymer/fullerene layer, which ranged from approximately 60 nm (high spin speeds) up to approximately

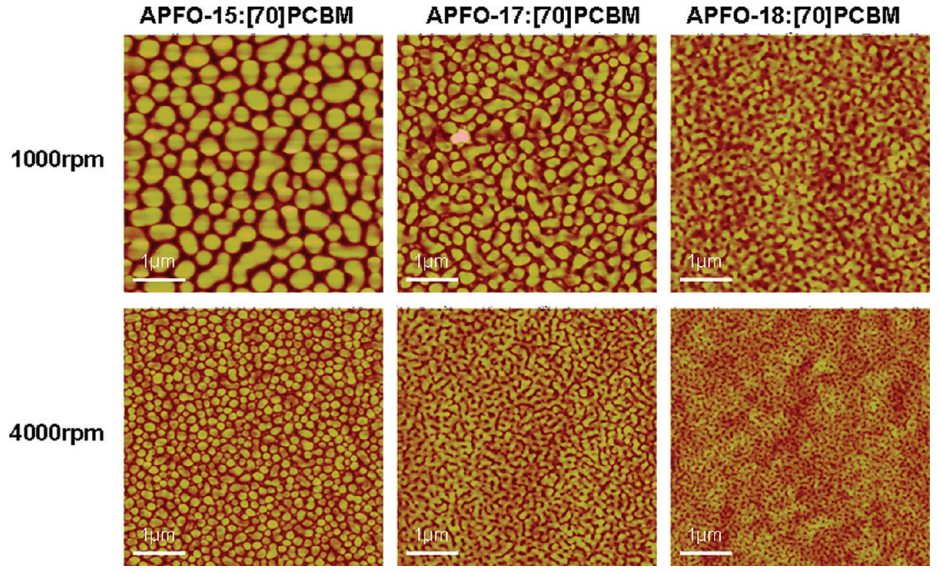

Figure 7. AFM images (height) of [70]PCBM:APFO mixtures, showing the influence of substitution and spin speed on the micrometer morphology.

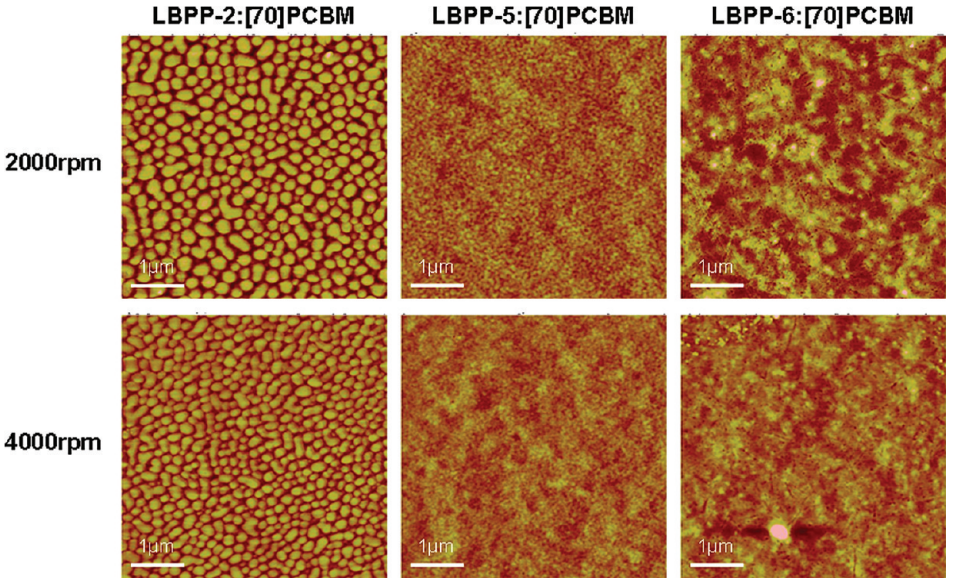

Figure 8. AFM images (height) of [70]PCBM:LBPP mixtures, showing the influence of substitution and spin speed on the micrometer morphology. The [70]PCBM:LBPP-6 mixture shows a phase separation different from LBPP-2 and 5, probably because of poor solubility and low molecular weight.

120 nm (low spin speeds). After deposition of LiF and aluminum (cathode), the resulting 24 different types of cells were characterized, and the results from the measurements are presented in Table 3. The results show that LBPP-6 has a remarkably poorer performance in solar cells using both [60]PCBM and [70]PCBM as electron acceptors. The reason for this is probably because of poor-quality films, which can be attributed to both low solubility and relatively low molecular weight.

With the exception of LBPP-6, a number of trends can be seen in the results from the photovoltaic characterization. Going from octyloxy substitution in APFO-15 to relatively short butoxy groups in APFO-17 and no substitution in APFO-18 increases the performance of the photovoltaic cells. The greatest changes are seen in short-circuit currents (J_{sc}) and power-conversion efficiencies (PCE), whereas the open-circuit voltage (V_{oc}) remains relatively constant. For the LBPP−polymers, a similar trend is observed for cells in which [70]PCBM is used as electron acceptor. However, for the corresponding cells containing [60]PCBM as electron acceptor, a decrease in performance is observed in going from LBPP-2 to LBPP-5. Furthermore, all polymer/fullerene mixtures show increased performances when the active layer is spin coated onto the PEDOT:PSS at high spin speed, resulting in thinner films. This trend is more pronounced for the [70]PCBM cells.

Although no extensive optimization work has been carried out, some of the devices show quite satisfactory performances. The best-performing cells are [70]PCBM devices, among which APFO-17, APFO-18, and LBPP-5 can be distinguished with PCE averages close to 3%. Furthermore, LBPP-5 shows high J_{sc}, well above 7.0 mA/cm^2. External quantum efficiencies (EQEs) and $I-V$ characteristics

for typical solar cells, fabricated using the highest spin speeds, are shown in Figures 4 and 5, respectively.

As mentioned earlier, the maximum V_{oc} obtainable in a photovoltaic device is related to the energy difference between the LUMO of the acceptor ([60]PCBM or [70]PCBM) and the HOMO of the polymer.[8,9] Using the results from the SWV measurements (from onset) this would give maximum open-circuit voltages of 1.3−1.5 V for the APFO polymers and approximately 1.0−1.1 V for the LBPP polymers. Comparing the actual voltages from devices with these values, a difference of approximately 0.5 V is seen for all polymers except LBPP-6, which shows a substantially lower V_{oc} in devices.

Morphology. Substitution and spin speed obviously have great impact on the properties of the cells, which is why atomic force microscopy (AFM) was employed to study morphological differences between the mixtures of electron acceptors and polymers. The AFM images of the [60]PCBM:polymer and [70]:polymer films are presented in Figures 6−8. From the images, a clear phase separation on the micrometer scale is seen in the [70]PCBM:polymer films, whereas the corresponding [60]PCBM:polymer films show a more smooth surface. When comparing the images of the [60]PCBM devices (Figure 6, fabricated at high spin speed), no major differences in morphology can be seen, which is in agreement with the rather small differences in solar-cell performance between the polymers.

In contrast, substantial differences in phase separation are seen for the [70]PCBM devices, and this is more pronounced for the APFO−polymers compared with the LBPP−polymers (Figures 7 and 8). These images show that, at the same speed of spin coating, shorter or no alkyloxy substitution results in a more disperse morphology with smaller domains. Furthermore, all [70]PCBM:polymer mixtures (once again excluding LBPP-6), fabricated at high spin speed, that is, faster evaporation of solvent and thinner films, show phase separation at a smaller length scale. Consequently, a clear correlation between the morphology and photovoltaic properties is seen for the [70]PCBM devices, where both shorter substitution on the low-band-gap segments and spin coating at a higher speed result in a more efficient device.

Mobility Measurements. To understand the differences in morphology and solar-cell performances, the mobilities of fullerene:polymer mixtures were studied. Electron and hole mobilities from FET measurements of all mixtures are presented in Figure 9. Mobilities are generally predicted to be larger in FETs than in solar cells. Experimentally it has been shown that there is roughly a factor of 8 between the mobilities of the two kinds of devices.[29] This factor has been taken into account in the mobility estimations shown in the figures.

All [70]PCBM:APFO blends show relatively low electron mobility and should thus show a strong thickness

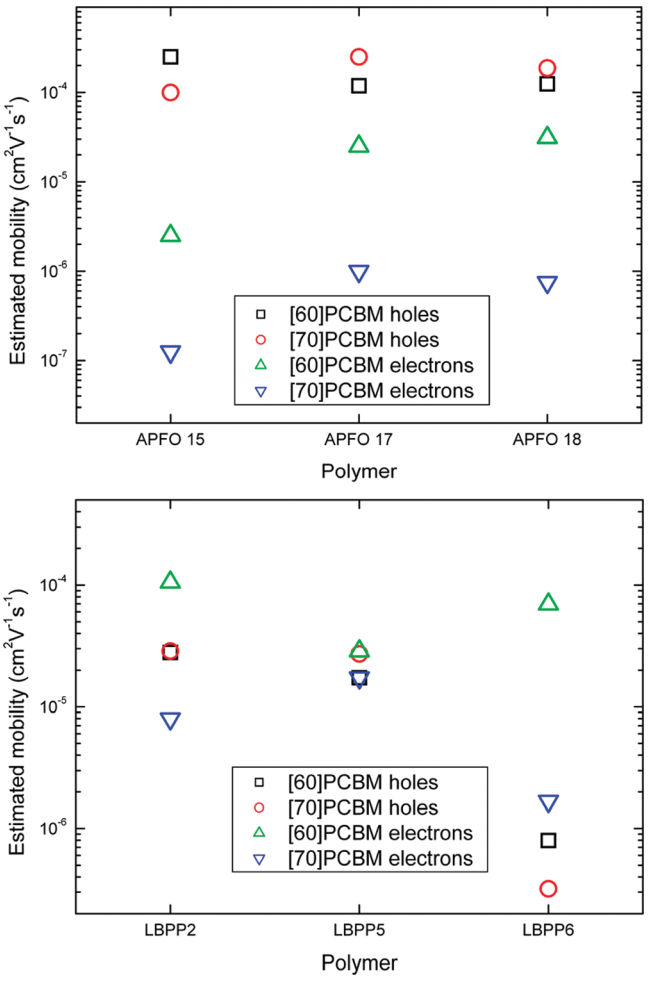

Figure 9. Estimated solar-cell mobilities from FET mobility measurements. Determination of both hole and electron mobilities are made on PCBM:polymer mixtures (4:1 by weight) and weighted with a factor of 1/8.

dependence, which is in agreement with the photovoltaic properties where the devices fabricated at high spin speed performs much better. Noticeable is the 10-fold increase in electron mobility in going from APFO-15 to APFO-17 (and APFO-18), that is, octyloxy to butoxy (or no) substitution, where also the greatest difference in morphology is seen. A similar correlation is seen when comparing LBPP-2 and LBPP-5, where [70]PCBM:LBPP-5 has a higher electron mobility and shows a smoother morphology on micrometer scale. Furthermore, the most balanced mobility, that is, the smallest difference between electron and hole mobility, is found in the [70]PCBM:LBPP-5 mixture, which is most likely the reason for the high short-circuit currents (J_{sc}) in these devices.

In addition, hole mobilities were measured on the pure polymers. For APFO-15, 17, and 18 these are 2×10^{-5}, 4×10^{-5}, and 6×10^{-5} $cm^2\,V^{-1}\,s^{-1}$, respectively. The corresponding values for LBPP-2, 5, and 6 are 4×10^{-5}, 6×10^{-5}, and 8×10^{-6} $cm^2\,V^{-1}\,s^{-1}$.

Conclusion

Six conjugated polymers were synthesized for solar cell applications, and their optical and electrochemical

(29) Andersson, L. M.; Zhang, F.; Inganas, O. *Appl. Phys. Lett.* **2006**, *89*, 142111/1–142111/3.

properties were evaluated. The polymers are of alternating polyfluorene (APFO) or polyphenylene (LBPP) type, containing low-band-gap monomers with different substituents. Within the groups, that is, APFOs and LBPPs, no great differences in optical absorption, electrochemical behavior, or FET mobility are seen for pure polymers. However, solar-cell performances, morphologies, and mobilities of polymers mixed with the acceptor [70]PCBM show substantial differences. In these films, it was observed that the polymers with long alkyloxy substituents, that is, APFO-15 and LBPP-5, tend to give rise to relatively large (up to > 500 nm) morphological domains. Smaller domains were seen in films of [70]PCBM mixed with the polymers with shorter alkoxy substituents. Hence, a clear correlation was seen between the local molecular structure and the macroscopic morphology on micrometer scale. Furthermore, films with smoother morphology not only show higher electron mobility but also show better solar-cell performance. A possible explanation for the phase-separation behavior could be the difference in polarity between the polymers and [70]PCBM, where polymers with long alkoxy chains are more hydrophobic, promoting phase separation. The morphological behavior can also be attributed to the excluded volume originating from the longer side chains. This prevents proper mixing both on the local molecular level and consequently also on a larger scale.

For the [60]PCBM mixtures no great differences could be seen in morphology on micrometer scale, but it is clear that substitution affects both mobility and photovoltaic properties.

One of the polymers, that is, LBPP-6, shows much lower molecular weight, low mobility in blends, and a morphology indicating precipitation of the polymer. In contrast and despite its relatively low molecular weight, APFO-18 does show one of the best performances in the devices. This comparison serves as a good example of when solubility and film-forming properties are the limiting factors for an efficient device.

Acknowledgment. We thank the Swedish Foundation for Strategic Research (SSF) for financial support through the Centre of Organic Electronics (COE).